J Mater Sci (2009) 44:998–1005
DOI 10.1007/s10853-008-3218-5

Unified description of martensite microstructure and kinetics

J. R. C. Guimarães · P. R. Rios

Received: 19 August 2008 / Accepted: 22 December 2008 / Published online: 13 January 2009

Abstract A quantitative metallography method is described to obtain size and number per unit volume of martensite units from linear intercept measurements. The entailed relationship between the number per unit volume of martensite plates and the volume fraction transformed is consistent with the autocatalytic nature of martensite. Application to the athermal and the isothermal martensite reactions allowed development of a unified microstructure-kinetic model. Validation of the model equations was achieved with data pertaining to FeNiC and FeNiMn alloys found in the literature. The apparent activation energy for propagation of isothermal martensite yielded by the transformation curve is compatible with the value obtained from the initial transformation rate. The defect redistribution process austenite/martensite established during the thickening of the plates has a crucial role in autocatalysis.

Introduction

The description of austenite transformation in steels has been a continuous endeavor of metallurgists [1]. Until the 1950s, when isothermal martensite was first observed [2, 3] the reaction was considered athermal. Since then, classical and non-classical concepts have been applied to rationalize the mechanism and to describe the transformation curve of martensite transformation [4]. Typically a martensite reaction proceeds by the nucleation of new units instead of by the growth of a few units. Moreover, the plates reach their final size nearly instantaneously, leading to the conclusion that nucleation controls martensite kinetics. Whereas "nucleation" would be barrier-less (athermal), martensite–austenite interface mobility requires overcoming short-range barriers which can be surmounted by thermal activation [4].

Extensive investigations, including computer modeling [5, 6], have propelled our understanding of martensite; however, certain aspects of martensite still benefit from the formal kinetics approach [7–12].

In a previous study [13], the present authors discussed the initial rate of martensite nucleation. In that study, we considered the temperature dependence of the number per unit volume of nucleation-related defects characteristic of particulate Fe–30.2 mass%Ni athermal transformation, as basis to model the initial reaction rate of isothermally transformed bulk Fe–23.2 mass%Ni–2.8 mass%Mn. In both alloys, plate martensite is formed at sub-zero temperatures. By considering the temperature dependence of the density of preferred nucleation sites for the initial nucleation of martensite inferred from athermal martensite formed in small particles [14], we described the onset isothermal martensite. Thus, the previous work provided an unified view of athermal and isothermal martensite reaction kinetics.

In this study we take this view as our starting point and develop it further to complete the unified description of the whole nucleation and growth kinetics of both athermal and isothermal plate martensite. In the first part of this study we advance a model that describes spatial aspects of

J. R. C. Guimarães · P. R. Rios (✉)
Escola de Engenharia Industrial Metalúrgica de Volta Redonda, Universidade Federal Fluminense, Av. dos Trabalhadores, 420, Volta Redonda, RJ 27255-125, Brazil
e-mail: prrios@metal.eeimvr.uff.br

J. R. C. Guimarães
Mal. Moura 338H/22C, Sao Paulo, SP 05641-000, Brazil

martensite plates in partially transformed austenite that allowed obtaining an analytical expression for martensite volume fraction as a function of number per unit volume. In the second part, using this new equation we derive the kinetic expressions. For convenience, we focus on martensite formed in FeNiC and FeNiMn alloys for which there are good amount of data already published.

Modeling number of martensite units per unit of volume

Fisher, Hollomon, and Turnbull

It is generally accepted that martensite is heterogeneous, that it proceeds by the addition of new units rather than by the growth of a few ones (in this sense the reaction is considered nucleation controlled). Therefore the evolution of the number per unit volume of the martensite units with the progress of the reaction is of considerable interest. Metallographic determination of number per unit volume is not trivial. Therefore, mathematical models have been proposed to accomplish that. Fisher et al. [15] were the first to propose such a model relating martensite volume fraction, V_v, to the number per unit volume, N_v, of the martensite units comprising the transformed volume. Figure 1a shows a typical martensite microstructure with 'zigzags' formation. The size of these plates is limited by other plates and/or austenite internal boundaries. Fisher et al. [15] modeled martensite microstructure in steel by assuming that the plates grow radially subdividing the austenite and thicken, thus transform a fixed fraction, m, of the initial austenite volume where they form, as illustrated in the schematic diagram of Fig. 1b. In Fig. 1b the hatched plates are those that form first.

$$\frac{dV_v}{dN_v} = m \cdot \frac{q(1 - V_v)}{1 + qN_v}, \quad (1)$$

where the volume of the next plate to form is given by dV_v/dN_v and q is the mean austenite grain volume. The quotient on the right-hand side of Eq. 1 expresses the average volume of austenite compartment after N_v martensite plates formed. The partitioning factor is equal to $1 + qN_v$.

Despite straightforward, the model has not been found always useful [16, 17]. Chen and Winchell [18] proposed a linear relationship between the mean diameter of a martensite plate to the mean-free intercept distance determined by the austenite grain boundaries and the midribs. However, this concept likewise Fisher's did not result in a good description of the microstructure. Consideration of autocatalysis and the heterogeneous spread of the reaction over the austenite grains led to the view that martensite

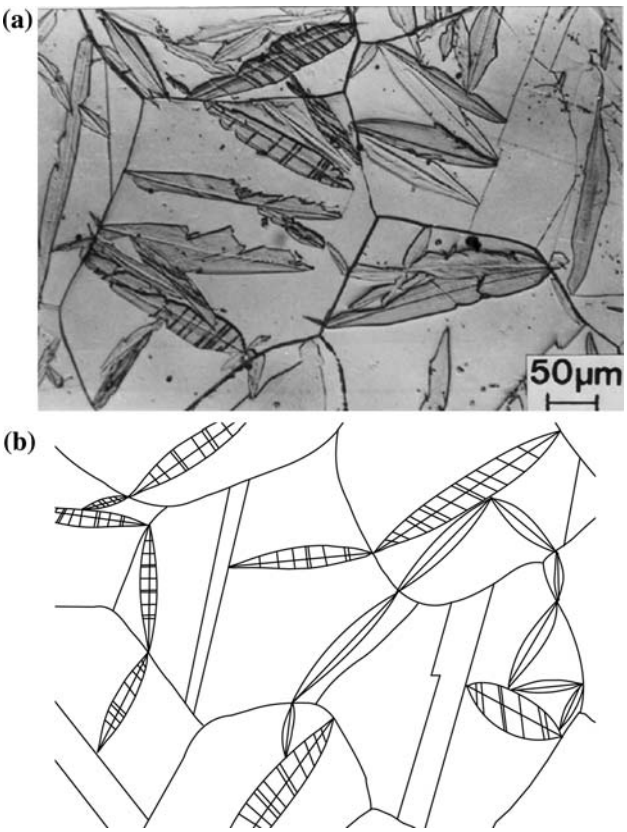

Fig. 1 **a** Typical martensite microstructure with 'zigzags' formation. The size of these plates is limited by other plates and/or austenite internal boundaries. **b** Schematic diagram based on **a**: the plates divide the austenite in "compartments"

mean-plate volume is invariant up to a significant volume fraction transformed [19].

New quantitative relationship

Martensite plates tend to form autocatalytic 'zigzags' of edging plates, as shown in Fig. 1a, to optimize the transfer of transformation strains to the matrix. Modeling requires simplifications. For that matter, it is generally accepted that the shape of a martensite plate approaches a slender oblate spheroid. The mid-plane of an oblate spheroid is a circle. As a consequence, the intersection of the mid-plane of a transformed spheroid with a metallographic section, revealed by the 'midrib', is a chord of the mid-plane. Considering the set of chords parallel to the midrib, the probable radius, r, of a spheroid with a midrib of length λ_c is given by [20]

$$r = \frac{2}{\pi} \cdot \lambda_c. \quad (2)$$

Since the diameter of a transformed spheroid's mid-plane is determined by impingement onto another spheroid

or onto a natural obstacle in the austenite, Fig. 1b, the mean midrib size, $\bar{\lambda}_c$, of the next generation of spheroids to form will estimate the mean austenite-free distance, $\bar{\lambda}_\gamma$, in the initial microstructure observed on a metallographic section,

$$\bar{\lambda}_\gamma = \frac{(1 - A_A)}{N_{L,m} + N_{L,\gamma\gamma}}, \tag{3}$$

where A_A is the areal fraction of martensite on that section, $N_{L,m}$ is number per unit length of martensite units and $N_{L,\gamma\gamma}$ is the number per unit length of austenite grains intercepted by a superimposed test line. $N_{L,m}$ and $N_{L,\gamma\gamma}$ can be equated, respectively, to half the number per unit length of martensite–austenite boundaries $P_{L,m,\gamma}$ and to the number of austenite boundaries $P_{L,\gamma\gamma}$ intercepted by the same test line. Recalling that the area per unit volume of a microstructure feature is calculated by the product [21] $S_v = 2P_L$, Eq. 3 can be recast

$$\bar{\lambda}_\gamma = \frac{4(1 - V_v)}{S_{v,m\gamma} + 2S_{v\gamma\gamma}}, \tag{4}$$

where the equivalence of areal fraction to volume fraction is acknowledged. Substitution of $\bar{\lambda}_\gamma$ for λ_c in Eq. 2 gives us the mean radius of the next generation of martensite plates

$$\bar{r} = \frac{8}{\pi} \frac{(1 - V_v)}{(S_{v,m\gamma} + 2S_{v,\gamma\gamma})}. \tag{5}$$

For a slender-isolated martensite plates $S_{v,m\gamma} \cong 2S_{v,m}$ where $S_{v,m}$ is the area per unit volume of midplane. However, since martensite plates impinge on each other as well onto grain and twin boundaries, $S_{v,m\gamma} = 2S_{v,m}(1 - V_v)$ and $S_{v,\gamma\gamma} = S_{v,\gamma}(1 - V_v)$. After using these two relationships into Eq. 5,

$$\bar{r} = \frac{4}{\pi(S_{v,m} + S_{v,\gamma})}. \tag{6}$$

Noteworthy, the mean intercept distance determined by midribs and grain plus twin boundaries is given by $\bar{\lambda}_i = 2/(S_{v,m} + S_{v,\gamma})$. Hence, it is implicit in Eq. 6 that the plate's mid-plane is the grain-partitioning vector. This is in line with the accepted view that martensite transformation is determined by the mid-plane propagation followed by thickening. $S_{v,\gamma}$ being a constant, the rate of change of area per unit volume of martensite mid-plane due to the next plate to form is

$$\frac{d(S_{v,m} + S_{v,\gamma})}{dN_v} = \pi\bar{r}^2 = \frac{16}{\pi}\left(S_{v,m} + S_{v,\gamma}\right)^{-2}. \tag{7}$$

Upon integration,

$$N_v = \frac{\pi}{48}\left[\left(S_{v,m} + S_{v,\gamma}\right)^3 - S_{v,\gamma}^3\right] \tag{8}$$

Equation 8 estimates N_v from linear intercept measurement. Important, Eq. 8 has *no adjustable parameters*. In addition, Eq. 8 bears a partitioning assumption compatible with martensite's touching midribs as seen in autocatalytic zigzags (Fig. 1a).

In order to validate Eq. 8, the data obtained with a high-purity Fe–31.9 wt%Ni–0.02 wt%C using Fullman's equations [22] were recovered from the original publication [23] by scanning and digitizing the graphs. All original data sources used in this study do not report error bars. However, the data were obtained using quantitative stereological techniques. Experience with this technique suggests that ±10% relative error is not a unreasonable estimate of errors associated with such measurements. Of course, in some cases one can obtain errors less than this, say ±5%, but in many cases errors can be larger, say ±20%, particularly for quantities that are derived from the ratio of two measured quantities. We believe ±10% relative error in the absence of data is a reasonable guide, and we inserted error bars corresponding to this to all data obtained by stereological techniques.

The compiled data, consolidated by reiteration to average out small variations, are plotted in Fig. 2. The straight line with unit slope passing through the origin describes the data, thus supporting the use of the model without any additional parameter. The correlation coefficient, R, of the data with respect to the line with unit slope was equal to 0.98.

It is apparent that the proposed method to obtain N_v from linear intercept determination yields results consistent with Fullman's disk analysis. However, whereas Fullman's requires measurements of individual plate dimensions and calculation of the reciprocal of such measurements, the method now proposed is more expeditious and does not require assuming disk-shaped plates. Moreover, the

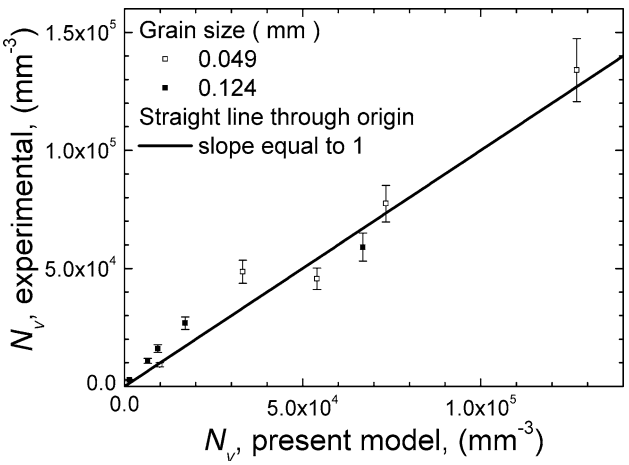

Fig. 2 Validation of the derived relationship between N_v and $S_{v,m}$, values of N_v obtained Fullman's disk analysis [22] are plotted against the values calculated using Eq. 8 for Fe–31.9 wt%Ni–0.02 wt%C with different austenite grain sizes (mean intercept length). A *straight line* through origin with slope one is also plotted as a reference

combination of Eqs. 6 and 8 allows expressing $\bar{r}$ as a function of N_v, yielding a relationship between V_v and N_v that may be used to develop an equation for the transformation curve, eventually. The volume of an oblate spheroid relates to its mid-plane's radius and semi-thickness as

$$v = \frac{4}{3}\pi r^2 c. \tag{9}$$

Substituting Eqs. 6 and 8 in Eq. 9 gives us

$$v = \frac{64}{3\pi}\frac{c}{S_{v,\gamma}^2}\left(1 + \frac{48}{\pi S_{v,\gamma}^3}N_v\right)^{-2/3}, \tag{10}$$

where v is the volume of the 'next' martensite plate to form from a microstructure that already containing N_v martensite plates yielding a volume fraction of martensite equal to V_v. Thus, as the 'next' martensite forms the increase in volume fraction of martensite with the number of plates, dV_v/dN_v, is equal to v

$$\frac{dV_v}{dN_v} = \frac{64}{3\pi}\frac{c}{S_{v,\gamma}^2}\left(1 + \frac{48}{\pi S_{v,\gamma}^3}N_v\right)^{-2/3}. \tag{11}$$

Equation 11 can be integrated after c is related to r. The simplest relationship is obtained by invoking a constant average aspect ratio, $\alpha = c/r$. Using Eqs. 6 and 8 yields

$$c = \frac{4\alpha}{\pi S_{v\gamma}}\left(1 + \frac{48}{\pi S_{v,\gamma}^3}N_v\right)^{-1/3}. \tag{12}$$

Substituting Eq. 12 in Eq. 11 gives us

$$\frac{dV_v}{dN_v} = \frac{256}{3\pi^2}\frac{\alpha}{S_{v,\gamma}^3}\left(1 + \frac{48}{\pi S_{v,\gamma}^3}N_v\right)^{-1}. \tag{13}$$

Integration of Eq. 13 obtains

$$V_v = \frac{16}{9\pi}\alpha\,\mathrm{Ln}\left(1 + \frac{48}{\pi S_{v,\gamma}^3}N_v\right). \tag{14}$$

Inspection of Eq. 14 shows that the sum between parentheses is analogous to Fisher's "$1 + qN_v$." The coefficient of N_v reflects the distinct assumptions of each model.

Experimental values of V_v and N_v characteristic of plate martensite formed in FeNiC alloys [24, 25], comprising austenite grain sizes (mean intercept) ranging from 0.026 to 0.434 mm, were recovered from the original publications as previously described. Regression analysis was carried out by plotting V_v against the right-hand side of Eq. 14 and obtaining α by linear regression. Table 1 depicts the results of the regression analysis of each set obtained from refs. [24, 25]; correlation coefficient, R, is high.

Figure 3 shows α plotted as a function of grain size. Except in one case, the values of α are within a narrow range of 0.2 to 0.3. The values of α obtained with the Fe–31.9 wt%Ni–0.02 wt%C data compare with the ratio of mean-thickness on mean-plate radius are shown in ref. [26].

Table 1 Regression results of obtained by best-fitting Eq. 14 to data from [24, 25]

	Grain size (mm)	α	R
Fe–31.9 wt%Ni–0.02 wt%C [25]	0.142	0.21	0.91
Fe–31.9 wt%Ni–0.02 wt%C [25]	0.048	0.27	0.85
Fe–32.3 wt%Ni–0.004 wt%C [24]	0.484	0.20	0.89
Fe–32.3 wt%Ni–0.004 wt%C [24]	0.121	0.29	0.94
Fe–32.3 wt%Ni–0.004 wt%C [24]	0.049	0.60	0.99

Grain size is the mean intercept length

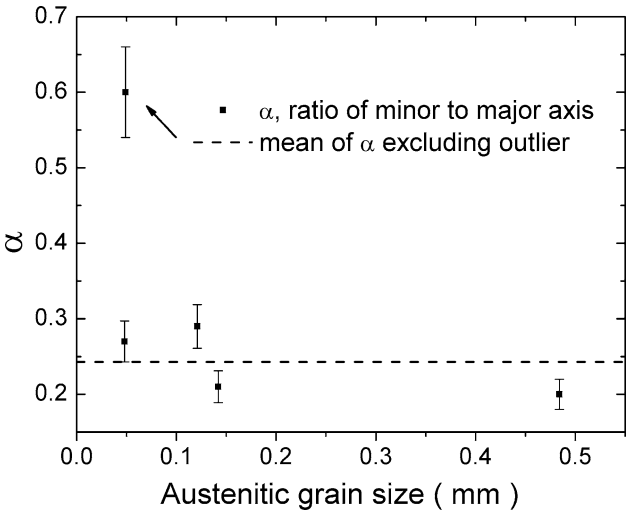

Fig. 3 Variation of the mean aspect ratio of martensite plates in FeNiC alloys [24, 25] as a function of the austenite grain size (mean intercept length)

However, the value of α for Fe–32.3 wt%Ni–0.004 wt%C with 0.049 mm grain size is twice as larger as any other value of α in the set, including that obtained with Fe–31.9 wt%Ni–0.02 wt%C of similar grain size (0.048 mm). The chemistry of the alloys is nearly the same, and the values N_v in either case were obtained after Fullman [22]. The outlier could have three reasons: (a) statistical error: owing to the small number of measurements the likelihood of obtaining an outlier is small but still possible; (b) it could be an experimental error: these data albeit not recent were carefully obtained and there is no reason to doubt the experimental proficiency of the authors; (c) it could represent a true physical effect: this would be unlikely and we could not support this with the limited amount of data available. Therefore, of the three possibilities, the most likely is that the outlier is a statistical effect.

Our approach is admittedly an approximation since α is likely to change with volume fraction. In fact, if the thickness of a martensite plate was solely related to the mid-plane radius, filling-in the untransformed austenite should require an infinite number of small plates. However, martensite plates usually form zigzags to relax accommodation strains, thus contributing to variation in α. The analytical description of α should improve the capability of the model, but it would require dealing with crystallographic aspects of martensite [27] which are beyond the scope of this article. Notwithstanding this approximation, the model now proposed provides a much better description of experimental data than Fisher's model equation 1 entails.

Martensite transformation curves

Inspection of plate martensite microstructure discloses several zigzag formations (Fig. 1), where plates are on a cooperative arrangement. Zigzags with distinct orientations are initiated by distinct initial nucleation events. Clearly the formation of a zigzag is concomitant with the propagation of midribs, which is generally accepted as the first stage of the transformation. As a consequence, the mechanism of autocatalysis that allows the cooperative formation of midribs can be considered to be mainly elastic. Operationally, thickening is the second operational stage of transformation. It results in the surrounding austenite being further strained. The resultant debris is expected to provide sites for the propagation of additional zigzags.

The kinetics of martensite nucleation has been interpreted by balancing site availability which comprises the initial sites, n_{v}^{i}, the autocatalytic sites assumed linearly dependent on the fraction transformed, and the ones propagated [28, 29]

$$n_{\mathrm{v}}^{\mathrm{T}} = \left(n_{\mathrm{v}}^{i} + pV_{\mathrm{v}} - N_{\mathrm{v}}\right)(1 - V_{\mathrm{v}}), \tag{15}$$

where p is the autocatalytic factor, $1 - V_{\mathrm{v}}$ is the exhaustion factor and the other terms were defined above. One issue regarding Eq. 15 is it assumes that the nucleation sites and events would be volumetric distributed in the material [30], whereas admittedly debris from accommodation strains would be generated in the surrounding austenite [31] before being preferentially absorbed into the martensite plate during thickening [6]. Since thickening cannot be envisaged to brush aside potential nucleation defects, the "defect redistribution" at the martensite–austenite interface must have a crucial role in autocatalysis.

To cope with this issue, we will assume that autocatalysis can be described by the product $a_{\mathrm{ac}}S_{\mathrm{m},\gamma}$ where $S_{\mathrm{m},\gamma}$ is the area of martensite–austenite interfaces and a_{ac} is a scale factor expressed per unit area. If the plates are described as slender oblate spheroids, $2S_{\mathrm{v},m}(1 - V_{\mathrm{v}})$ where $S_{\mathrm{V,m}}$, the area of plates' mid-plane per unit volume of material, can be substituted for $S_{\mathrm{v,m}\gamma}$, yielding

$$n_{\mathrm{v,ac}}^{\mathrm{T}} = 2S_{\mathrm{v},m}(1 - V_{\mathrm{v}})a_{\mathrm{ac}}. \tag{16}$$

Analysis of small particles transformation data [14] has indicated that *the effect of temperature on the initial nucleation site density* can be expressed as

$$n_{\mathrm{v}}(T) = n_{\mathrm{v}}^{0}\frac{\Delta S}{k}\frac{T^{*} - T}{T}, \tag{17}$$

where ΔS is the entropy change, k the Boltzmann constant, T^{*} the highest temperature at which the reaction is first observed, and T the actual reaction temperature [13]. Considering that autocatalysis is overwhelming since inception, $n_{\mathrm{v,ac}}^{\mathrm{T}}$ can be substituted for n_{v}^{0}, yielding

$$\mathrm{d}N_{\mathrm{v}} = n_{\mathrm{v,ac}}^{\mathrm{T}}\frac{\Delta S}{k}\frac{T^{*} - T}{T}(1 - V_{\mathrm{v}})R_{\xi}\,\mathrm{d}\xi, \tag{18}$$

where R_{ξ} expresses a rate constant and ξ is the experimental variable.

Noteworthy, $1 - V_{\mathrm{v}}$ in Eq. 18 accounts for exhaustion. However, in Eq. 16, $1 - V_{\mathrm{v}}$ accounts for plates' impingement. Therefore, substituting Eq. 16 into Eq. 18 gives us

$$\mathrm{d}N_{\mathrm{v}} = 2S_{\mathrm{v,m}}a_{\mathrm{ac}}(1 - V_{\mathrm{v}})^{2}\frac{\Delta S}{k}\frac{T^{*} - T}{T}R_{\xi}\,\mathrm{d}\xi. \tag{19}$$

The resultant transformation curve is obtained by combining Eqs. 8, 14, and 19

$$\int \frac{9\pi e^{\frac{9\pi V_{\mathrm{v}}}{16\alpha}}\mathrm{d}V_{\mathrm{v}}}{16\alpha\left(e^{\frac{3\pi V_{\mathrm{v}}}{16\alpha}} - 1\right)(1 - V_{\mathrm{v}})^{2}} = \frac{96a_{\mathrm{ac}}}{\pi S_{\mathrm{v}}^{2}}\int \frac{\Delta S}{k}\frac{T^{*} - T}{T}R_{\xi}\,\mathrm{d}\xi. \tag{20}$$

In order to complete modeling the transformation curve, the propagation of a nucleation defect must be looked at. Propagation has been envisaged to be thermally activated or athermal. The later is normally identified with a temperature-dependent transformation curve that begins at certain, M_{s}, temperature *without contribution of thermal activation*. In order to describe the athermal mode we *formally* set $\xi = T$ (temperature), and R_T is the "rate" with respect to temperature, not time, at which nucleation event occurs. R_T is expressed per Kelvin. An athermal nucleation event takes place instantaneously. In the isothermal case $\xi = t$ (time), R_t will be described as usual, by an Arrhenius exponential [4, 32, 33].

Athermal martensite

The athermal kinetics is typified by the martensite transformation in quench-hardened steel. However, to validate the model, Eq. 20, for athermal propagation, data obtained

with high-purity Fe–31.9 wt%Ni–0.02 wt%C [25] and with Fe–32.3 wt%Ni–0.004 wt%C [24] were used. The procedure for data acquisition used here was already described before. Numerical integration was accomplished by applying the trapezoidal rule. Since the integrand on the left-hand side of Eq. 20 diverges at $V_v = 0$, integration was carried out between the martensite start temperature, M_s and T

$$\int_{V_{v,M_s}}^{V_v} \frac{9\pi e^{\frac{9\pi}{16\alpha}V_v} dV_v}{16\alpha\left(e^{\frac{3\pi}{16\alpha}V_v} - 1\right)(1 - V_v)^2} = A\frac{\Delta S}{k}R_T\left[\left(M_s \,\mathrm{Ln}\frac{M_s}{T}\right) - (M_s - T)\right] \quad (21a)$$

or

$$I(V_v) = AR_T T(T), \quad (21b)$$

where $I(V_v)$ stands for the integral on the left-hand side of Eq. 21a, $T(T)$ represents the function of the temperature on the right-hand side of Eq. 21a, and $A = \frac{96a_{ac}}{\pi S_v^2}$.

Table 2 summarizes the results obtained by best-fitting Eqs. 21a and 21b to data from refs. [23, 24]. Values of α from Table 1 and $\Delta S/k \cong 0.67$ [32] were used. The correlation coefficient, R, is high for all grain sizes. The slope of the fitted lines, values of AR_T are given in Table 2, increases with increasing grain size. Figure 4 shows the plot of best-fitted and experimental results obtained for grain sizes of 0.048 and 0.484 mm, thus providing a visual confirmation of the high correlation coefficients reported in Table 2.

Isothermal martensite

The initial rate of isothermal martensite in FeNiMn has been properly described by assuming single activated kinetics [13]. Therefore, $\xi = t$ (time) and $R_t = v\exp(-E_p/kT)$ where E_p is an apparent activation energy and $v = 10^{13}$ s^{-1}, T the temperature, and k the Boltzmann constant. Substituting that expression of R_t into Eq. 20

Table 2 Regression results obtained by best-fitting Eqs. 21a and 21b to data from [24, 25] for Fe–Ni–C alloys

S_v (mm^{-1})	Grain size (mm)	α	AR_T (K^{-1})	R
4.13 [24]	0.484	0.20	387	0.99
14.1 [25]	0.142	0.21	571	0.96
40.8 [25]	0.048	0.27	31	0.96
76.5 [25]	0.026	0.44[a]	9	0.97

Grain size is the mean intercept length

[a] For the 0.026 mm α was obtained directly from the best-fitted parameters

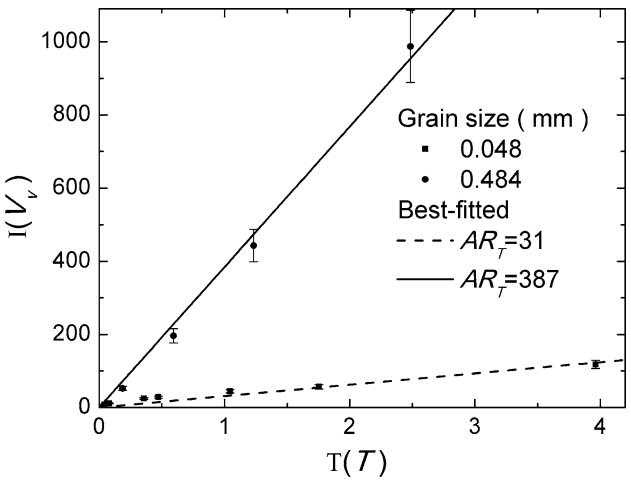

Fig. 4 Description of athermal transformation in FeNiC data [24, 25] with different austenite grain size (mean intercept length) using the proposed model Eqs. 21a and 21b

$$\int_{V_{v,1}}^{V_v} \frac{9\pi e^{\frac{9\pi}{16\bar{\alpha}}V_v} dV_v}{16\bar{\alpha}\left(e^{\frac{3\pi}{16\bar{\alpha}}V_v} - 1\right)(1 - V_v)^2} = A\int_{t_1}^{t} \frac{\Delta S}{k}\frac{T^* - T}{T} v\exp\left(-\frac{E_p}{kT}\right)dt \quad (22)$$

or

$$\int_{V_{v,1}}^{V_v} \frac{9\pi e^{\frac{9\pi}{16\bar{\alpha}}V_v} dV_v}{16\bar{\alpha}\left(e^{\frac{3\pi}{16\bar{\alpha}}V_v} - 1\right)(1 - V_v)^2} = A\frac{\Delta S}{k}\frac{T^* - T}{T}\exp\left(-\frac{E_p}{kT}\right)v(t - t_1). \quad (23)$$

Defining B as

$$B = A\frac{\Delta S}{k}\frac{T^* - T}{T}\exp\left(-\frac{E_p}{kT}\right). \quad (24)$$

Equation 24 can be written in a more compact form

$$I(V_v) = B(v\Delta t), \quad (25)$$

where $I(V_v)$ stands for the integral on the left-hand side of Eq. 23, $v\Delta t = v(t - t_1)$, represents the function of the time on the right-hand side of Eq. 23. In order to validate the model, Eqs. 23 through 25, we used the data from isothermally transformed similar FeNiMn with different grain sizes, 0.015 mm from ref. [29] and 0.048 mm grain size from ref. [34]. These published data were recovered and processed as described in the foregoing, ad hoc applying Eq. 14. Integration was performed in the interval $[t_1, t]$ where t_1 is defined by the first non-zero meaningful volume fraction reading, $V_{v,1}$. A parametric least square procedure on α was used to fit the data with Eq. 23. Table 3 summarizes the results obtained by best-fitting Eq. 23 to

Table 3 Regression results obtained by best-fitting Eq. 25 to experimental data on isothermal martensite

T (K)	α	c/r	B	R
Ghosh and Raghavan [34] for a Fe–Mn–Ni alloy with a 0.048 mm grain size				
77	0.10	0.04–0.06	9.67×10^{-16}	0.98
133	0.044	0.050–0.07	1.75×10^{-13}	0.96
143	0.044	0.06–0.07	3.39×10^{-13}	0.99
163	0.029	0.06–0.08	1.00×10^{-9}	0.99
173	0.024	0.07–0.08	1.27×10^{-9}	0.98
193	0.074	~0.08	4.84×10^{-16}	0.95
203	0.024	NA	3.40×10^{-16}	0.97
Pati and Cohen [29] for a Fe–Mn–Ni alloy with a 0.015 mm grain size				
77	0.035	NA	2.09×10^{-16}	0.92
90	0.098	NA	1.26×10^{-15}	0.99
133	0.11	NA	1.24×10^{-14}	0.99
148	0.08	NA	4.10×10^{-14}	0.99
158	0.12	NA	8.44×10^{-15}	0.99
168	0.08	NA	3.14×10^{-15}	0.99
183	0.13	NA	5.65×10^{-16}	0.99
193	0.06	NA	2.35×10^{-16}	0.99

Grain size is the mean intercept length

data from refs. [29, 34]. The correlation coefficient, R, is high for all transformation temperatures. The values of α obtained with the Gosh and Raghavan [34] data are in reasonable agreement with the average aspect ratio (c/r) of the martensite plates determined by optical metallography, but α does not vary with temperature as conspicuously as the experimental values of aspect ratio in ref. [34]. Noteworthy the values of α obtained with the FeNiC alloys are much larger than the ones typical of the FeNiMn. Figure 5 shows the good agreement of best-fitted and experimental results obtained for a range of temperatures, the lowest 77 K and the highest 203 K. Other temperatures are not shown because of the large-scale difference in the values of B, but the agreement is, of course, similar at all temperatures as they all have a high correlation coefficient (see Table 3).

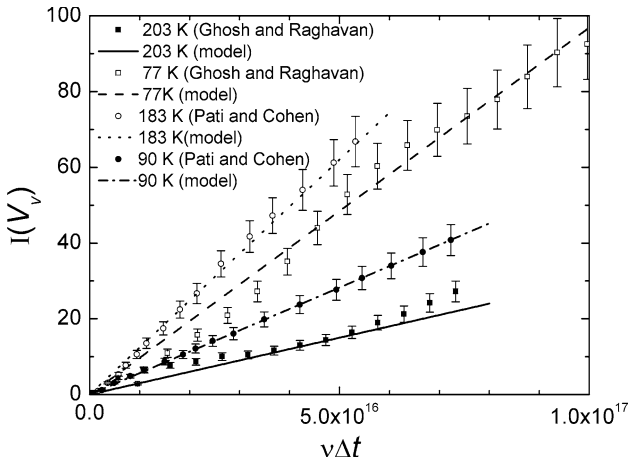

Fig. 5 Description of isothermal FeNiMn data [29, 34] with different austenite grain sizes (mean intercept length) at different temperatures, using the proposed model Eqs. 25–27

Discussion

The slope of the fitted lines (values of B in Table 3) passes through a maximum as the transformation temperature decreases from 203 to 77 K. This reflects the "C" curve behavior of isothermal martensite transformation kinetics. Therefore the values of B in Table 3 were used in a Arrhenius graph (data not shown) to obtain the values of the apparent activation energy for the isothermal reaction, E_p, and of the parameter, A. T^* was used as the adjusting parameter, and $\Delta S/k \cong 0.67$ [30].

$$\ln\left(\frac{BkT}{(T^* - T)\Delta S}\right) = \ln(A) - \frac{E_p}{kT}. \quad (26)$$

Using, Gosh and Raghavan data one obtains E_p, 2.4×10^{-20} J per event with $T^* \cong 203$ K but the correlation coefficient was only fair, $R = 0.60$ because the value of B at 193 K appears out of context. However with Pati and Cohen data [29] one obtains $R = 0.90$ and nearly the same value of E_p, 1.1×10^{-20} J per event. Moreover, both values of E_p are in the range of calculated values of martensite nucleation energy [4] as well as it is within an order of magnitude of the 7.5×10^{-21} J per event determined from the initial reaction rate [13].

The values of A determined with Eq. 26 are 2.6×10^{-6} (Ghosh and Raghavan data, 0.048 mm grain size) and 4.0×10^{-12} (Pati and Cohen data, 0.015 mm grain size). The parameter A relates to autocatalysis and to grain size

through the square of S_V, $A = 96a_{ac}/\pi S_V^2$. The effect of grain size, from 0.048 to 0.015 mm, or S_V^2 is about an order of magnitude and on its own cannot explain the large variation in A. Most of the variation is explained by the large change in the values of the autocatalytic parameter a_{ac}, which decreases from 1.4×10^{-4} to 2.3×10^{-9} mm^{-2} as the grain size decreases from 0.048 to 0.015 mm.

However, this large difference may be fortuitous, relating to the different values of the correlation coefficient above reported. On the other hand, it is noteworthy that the size of isothermal martensite plates in the FeNiMn is also limited by other obstacles than grain and twin boundaries in the austenite [34–36]. This suggests a significant defect redistribution at the martensite–austenite, which implies in a larger value of the autocatalytic parameter a_{ac}, in comparison with a bursting FeNiC alloy. Martensite plates in FeNiC exhibit fast radial growth till stopped by other plates or by austenite's grain and twin boundaries. Unfortunately, further comparison is hindered because R_T is not known, and could not be independently obtained at this time. This is an issue that deserves further investigation.

Summary and conclusions

A quantitative metallography method was advanced to obtain size and number per unit volume of martensite units from linear intercept measurements. The model entails a description of the relationship between number per unit volume of martensite and volume fraction transformed consistent with the autocatalytic nature of plate martensite. The model equation, Eq. 14, likewise, the Fisher's partitioning model, bears one fitting parameter.

Application of the model to the athermal and the isothermal martensite reactions allowed to develop a unified microstructure-kinetic model. Validation of the equations derived for the transformation curves was achieved with available experimental data pertaining to FeNiC, FeNiMn alloys found in the literature.

The defect redistribution process established during the thickening of the plates has a crucial role in autocatalysis.

The apparent activation energy for propagation of isothermal martensite obtained from the transformation curve is compatible (within one order of magnitude) with the value obtained from the initial transformation rate, supporting the extension of the kinetic concepts based upon the initial transformation rate of martensite, ref. [13], to the overall transformation curve.

In summary, by developing a new relationship between the number of martensite plates per unit of volume and the area of the midrib plane and combining it with the previous model for martensite initial reaction rate [13] while refocusing autocatalysis, a new model has been proposed here that satisfactorily explains both athermal and isothermal martensite transformation kinetics.

Acknowledgements One of the authors (P.R. Rios) is grateful to Conselho Nacional de Desenvolvimento Científico e Tecnológico, CNPq, and to Fundação de Amparo à Pesquisa do Estado do Rio de Janeiro, FAPERJ, for his financial support. Thanks are due to Chris Hoffman (RMC Inc.) and to Professor H. Goldenstein (USP-SP) for their valuable assistance with the bibliography.

References

1. Zhao J-C, Notis MR (1995) Mater Sci Eng R 15:135
2. Kurdjumov GV, Maximova OP (1948) Dokl Akad Nauk SSSR 61:83
3. Kurdjumov GV, Maximova OP (1950) Dokl Akad Nauk SSSR 73:95
4. Olson GB, Cohen M (1985) Principles of martensitic transformation, frontiers in materials technologies. Elsevier, Amsterdam, p 43
5. Ping X, Morris JW Jr (1993) Metall Trans A24:1281
6. Levitas VI, Idesman AV, Olson GB, Stein E (2002) Philos Mag 82:429
7. Harris WJ, Cohen M (1949) Trans AIME 180:447
8. Koistinen DP, Marburger RE (1959) Acta Metall 7:59
9. Rios PR, Guimarães JRC (2007) Scr Mater 57:1105
10. Rios PR, Guimarães JRC (2008) Mater Res 11:103. doi:10.1590/S1516-14392008000100020
11. van Bohemen SMC, Sietsma J, Hermans MJM, Richardson IM (2003) Acta Mater 51:4183
12. Guimaraes JRC (2008) Mater Sci Eng A 476:106
13. Guimarães JRC, Rios PR (2008) J Mater Sci. doi:10.1007/s10853-008-2753-4
14. Cech RE, Turnbull D (1956) Trans AIME 206:124
15. Fisher JC, Hollomon JH, Turnbull D (1949) AIME Trans 185:691
16. McMurtrie MG, Magee CL (1970) Metall Trans 1:3185
17. Mendiratta MG, Krauss G (1972) Metall Trans 2:1755
18. Chen WYC, Winchell PG (1976) Metall Trans A 7:1177
19. Magee CL (1970) In: Aaronson HI (ed) Phase transformations. ASM, Metals Park, p 115
20. Coleman R (1989) Can J Stat 17:27
21. Russ JC, Dehoff RT (2000) Practical stereology, 2nd edn. Kluwer Academic, New York
22. Fullman RL (1953) Trans AIME 197:447
23. Guimarães JRC (1982) In: Aaronson HI et al (eds) Solid-solid phase transformations. TMS AIME, Warrendale, p 1415
24. Lin MF, Olson GB, Cohen M (1992) Metall Trans A 23:2987
25. Guimarães JRC, Saavedra A (1985) Metall Trans A 16:329
26. Guimarães JRC, Gomes JC (1979) In: Owen WS (ed) ICOMAT-1979 proceedings. MIT Press, Cambridge, p 59
27. Kelly PM (2006) Mater Sci Eng A 438:43
28. Raghavan V, Entwisle AR (1965) Physical properties of martensite and bainite. ISI special report 93. Iron and Steel Institute, London, p 30
29. Pati SR, Cohen M (1971) Acta Metall 19:1327
30. Christian JW (1965) Physical properties of martensite and bainite. ISI special report 93. Iron and Steel Institute, London, p 43
31. Entwisle AR (1965) Physical properties of martensite and bainite. ISI special report 93. Iron and Steel Institute, London, p 43
32. Kaufman L, Cohen M (1958) Prog Met Phys 7:165
33. Borgenstam A, Hillert M (1997) Acta Mater 45:651
34. Ghosh G, Raghavan V (1986) Mater Sci Eng 79:223
35. Ghosh G (1988) Mater Sci Eng A 101:213
36. Guimaraes JRC (2008) Mater Sci Technol 24:843